Received: 29 April 2019 | Revised: 13 November 2019 | Accepted: 5 December 2019

DOI: 10.1111/ejss.12927

SHORT COMMUNICATION

European Journal of Soil Science WILEY

# Permafrost soil complexity evaluated by laboratory imaging Vis-NIR spectroscopy

**Carsten W. Mueller**[1] | **Markus Steffens**[2] | **Henning Buddenbaum**[3]

[1]Research Department Ecology and Ecosystem Management, Chair of Soil Science, Technical University of Munich, Freising-Weihenstephan, Germany

[2]Department of Soil Sciences, Research Institute of Organic Agriculture FiBL, Frick, Switzerland

[3]Regional and Environmental Sciences, Environmental Remote Sensing and Geoinformatics, University of Trier, Trier, Germany

**Correspondence**
Carsten W. Mueller, Chair of Soil Science, Technical University of Munich, Freising-Weihenstephan, 85354, Germany.
Email: carsten.mueller@wzw.tum.de

**Funding information**
Deutsche Forschungsgemeinschaft, Grant/Award Numbers: MU 3021/2-1, MU 3021/8-1; Deutsches Zentrum für Luft- und Raumfahrt, Grant/Award Number: 50 EE 1530; National Science Foundation, Grant/Award Number: 0852036

## Abstract

The biogeochemical functioning of soils (e.g., soil carbon stabilization and nutrient cycling) is determined at the interfaces of specific soil structures (e.g., aggregates, particulate organic matter (POM) and organo-mineral associations). With the growing accessibility of spectromicroscopic techniques, there is an increase in nano- to microscale analyses of biogeochemical interfaces at the process scale, reaching from the distribution of elements and isotopes to the localization of microorganisms. A widely used approach to study intact soil structures is the fixation and embedding of intact soil samples in resin and the subsequent analyses of soil cross-sections using spectromicroscopic techniques. However, it is still challenging to link such microscale approaches to larger scales at which normally bulk soil analyses are conducted. Here we report on the use of laboratory imaging Vis–NIR spectroscopy on resin embedded soil sections and a procedure for supervised image classification to determine the microscale soil structure arrangement, including the quantification of soil organic matter fractions. This approach will help to upscale from microscale spectromicroscopic techniques to the centimetre and possibly pedon scale. Thus, we demonstrate a new approach to integrate microscale soil analyses into pedon-scale conceptual and experimental approaches.

## Highlights

- Quantification of soil constituents using Vis-NIR spectroscopy.
- New approach to use resin embedded soil core sections with intact structure.
- Reproducible quantification of soil constituents important for soil carbon storage.
- Vis-NIR as promising tool for upscaling from microscale to pdeon scale.

**KEYWORDS**

Alaska, HySpex, mineral associated organic matter, occluded particulate organic matter, particulate organic matter, pedogenic iron oxides, supervised image classification

Soil functions are driven by microscale processes and thus there is a need for analytical techniques to directly study physical, biological and chemical processes in intact soil samples (Baveye et al., 2018). To analyse microscale biogeochemical interfaces for their chemical and/or isotopic composition or the distribution of microbial cells in intact soil samples, it is mandatory to use approaches that assure an undisturbed soil structure. A

widely used technique to preserve soil structures is the embedding of soil samples (from aggregates up to complete soil cores) in resin and the subsequent production of soil cross-sections (Eickhorst & Tippkoetter, 2008; Herrmann et al., 2007; Kubiena, 1938). Although the use of epoxy or polyester resin for soil impregnation and thus soil structure preservation introduces possible artefacts via the redistribution of soluble compounds or the dilution of isotopic enrichments, it is up to now the only way to correlatively combine 3D soil physical structure measurements (e.g., μCT) with 2D imaging approaches, for example the localization of distinct microbial groups (e.g., fluorescence in situ hybridization) and elemental distribution (Eickhorst & Tippkoetter, 2008; Juyal et al., 2019; Schlueter, Eickhorst, & Mueller, 2019). However, because all of these techniques reveal structures at a very fine scale, the field of view is very restricted (Eickhorst & Tippkoetter, 2008; Herrmann et al., 2007; Kravchenko et al., 2019; Mueller et al., 2013; Steffens et al., 2017) and therefore upscaling from the aggregate to soil core or even to the pedon scale is of crucial importance but also complicated. Thus, there is a clear deficit in correlative approaches that link microscale measurements with soil structures and constituents at the mm to cm scale.

To close such spatial gaps, we think that spectroscopic imaging approaches can be one way to quantify soil constituents and thus biogeochemical interfaces from the aggregate to the pedon scale. A promising approach to evaluate complex intact soil structures was demonstrated by Steffens and Buddenbaum (2013), who used visible to near infrared (Vis–NIR) laboratory imaging spectroscopy (imVisIR). The authors used the method on dried intact soil profiles and were able to differentiate soil elemental and structural features in mineral and organic soils. Because a variety of techniques that aim to analyse intact soil structures at the microscale make use of resin-embedded soil sections (Eickhorst & Tippkoetter, 2008; Herrmann, Ritz, et al., 2007; Juyal et al., 2019; Mueller et al., 2013; Nunan et al., 2001; Rodionov et al., 2019; Schlueter et al., 2019; Vidal et al., 2018), the use of imVisIR on these sections would enable upscaling and correlation with bulk soil features (Manß, Hilgers, Buddenbaum, & Stanjek, 2017). However, because, up to now, imVisIR has been used in soil science exclusively to analyse natural non-embedded soil, it was not clear if the use of embedding resin would hamper the classification and thus the quantification of microscale soil structures.

Here, we report on the use of imVisIR on epoxy resin-embedded Cryosol soil core sections described in Mueller et al. (2017). Permafrost-affected soils are highly complex in structure and also tremendously important for global carbon storage (Mueller et al., 2015; Schuur et al., 2008; Schuur et al., 2015; Tarnocai et al., 2009; Zimov, Schuur, & Chapin, 2006); thus, they make a well-suited and relevant model system to test this application of imVisIR. Comparable to temperate soils, distinct physical soil organic matter fractions are key for long-term carbon storage in permafrost affected soils (Gentsch et al., 2015; Mueller et al., 2015). At the microscale it was even possible to demonstrate the importance of specific fine soil structures (e.g., particulate organic matter (POM)) in Cryosols for the formation of microaggregates in the vicinity of decaying plant residues (Mueller et al., 2017). Interestingly, old carbon, which in studies on temperate soils is often linked to organo-mineral associated organic matter (MOM) or small occluded POM, was demonstrated to be as vulnerable to soil warming as young organic matter in Arctic soils (Vaughn & Torn, 2019). The interaction of plant residues, microbial-derived extracellular polymeric substances and the surrounding soil minerals in the formation of aggregated soil structures in Arctic soils was shown by using scanning electron microscopy and nanoscale secondary ion mass spectrometry (NanoSIMS) (Mueller et al., 2017). Here we use the exact same Cryosol thin section as in Mueller et al. (2017) to demonstrate the feasibility of imVisIR to quantify soil constituents important for soil organic matter (SOM) storage in embedded and sectioned soil samples. Our approach allows for the determination of soil structural domains representing specific biogeochemical interfaces and thus areas that may act as hot spots for soil organic carbon stabilization, microbial activity, nutrient sorption and cycling.

We made use of samples taken at the Barrow Peninsula, on the Arctic Coastal Plain, in April 2010 (Mueller et al., 2015). From a number of soil cores, subsections were gently thawed, stepwise dried using a row of graded acetone to water mixtures, embedded in an epoxy resin (Araldite 502) and subsequently sectioned and polished as described by Mueller et al. (2017). In Mueller et al. (2017) one subsection called B1-5U-2 was analysed in detail using reflectance light microscopy, scanning electron microscopy and NanoSIMS. Here, we describe the analyses of imVisIR datasets of this subsection and another subsection from the same horizon called B1-5U-1. The analysed soil contains a mineral matrix consisting of quartz grains and fine sand, iron oxides and POM in several levels of decomposition (Mueller et al., 2017). According to Mueller et al. (2017), the bulk soil contained 8.4 wt% POM and 91.6 wt% mineral constituents (Table 1). The studied Cryosol organic carbon (OC) storage was distributed into 36.8% OC stored as POM and 63.2% OC stored as mineral-associated OM, which is in line with samples of various other cores from the same sampling campaign (Mueller et al., 2015).

Hyperspectral images of the soil core subsections were recorded with a HySpex VNIR-1600 hyperspectral

**TABLE 1** Frequency of information classes in both resin-embedded drill core subsections; comparison with amount of particulate (POM) and mineral-associated organic matter (MOM) from density fractionation of the bulk soil (as given in Mueller et al., 2017)

| | | Vis–NIR image classification | | | | | SOM fractionation |
|---|---|---|---|---|---|---|---|
| | | B1-5U-2 | | B1-5U-1 | | Mean | Amount |
| Assigned SOM | Information classes | N pixels | % | N pixels | % | % | % |
| Unclassified | | 918 | 0.7 | 44 | 0.03 | | |
| POM | Fresh POM | 3281 | 2.5 | 2858 | 2.2 | 9.29 | 8.38 |
| | Undecomposed POM | 2364 | 1.8 | 171 | 0.13 | | |
| | Decomposed POM | 4583 | 3.5 | 2087 | 1.6 | | |
| | Highly decomposed POM | 5257 | 4.0 | 3714 | 2.9 | | |
| MOM | Fe-oxides | 3456 | 2.6 | 4249 | 3.3 | 90.35 | 91.62 |
| | Mineral matrix | 111921 | 84.9 | 116258 | 89.9 | | |

Abbreviation: SOM, soil organic matter.

line scanner (Norsk Elektro Optikk, Skedsmokorset, Norway). The camera was equipped with a 30-cm close-up lens and set up in a laboratory frame 30 cm above the samples, with light sources illuminating the samples from a distance of about 35 cm and at an angle of about 45° in front of and behind the camera. The samples were placed on a translation stage that moved the samples under the camera. In the direction perpendicular to the movement of the sample (across-track direction), the camera recorded 1,600 pixels with a field of view of 17°. The instantaneous field of view for each pixel was 0.18 mrad across the track and 0.36 mrad along the track. The area that was recorded by the camera from a 30-cm distance was 10 cm wide, so that a single pixel was 62.5 μm wide. The subsections (disks) have a diameter of 2.5 cm, so they cover circles with ca. 400 pixel diameters in the hyperspectral images. The camera records 160 spectral bands in the spectral range of 410 to 990 nm, with a spectral sampling distance of 3.7 nm.

Achieving a high signal-to-noise ratio (SNR) is always a challenge in imaging spectroscopy. Usually, a white reference plate with nearly 100% reflectance is recorded with the object of interest to facilitate transformation from the recorded radiance to reflectance (Buddenbaum & Steffens, 2011; Rogass et al., 2017; Steffens & Buddenbaum, 2013). The reflectance factor of the target can be calculated as the ratio of radiances from the target and the reference, multiplied by the reflectance of the reference (Schaepman-Strub, Schaepman, Painter, Dangel, & Martonchik, 2006). Because the drill core disks are rather dark with a mean Vis–NIR reflectance of just 4%, adjusting the exposure time to the white reference would have led to a very low signal level for the disks. Instead, the reflectance of a dark brown cardboard plate was carefully measured against the white reference and then the cardboard plate was used as the reflectance standard. This way, a much higher exposure time could be set, leading to a higher SNR. When all target pixels are corrected with the same reference spectrum, small wavelength shifts across the field of view of the camera can cause faulty spectra (Buddenbaum, Watt, Scholten, & Hill, 2019). To avoid this, reflectance factors were calculated for each image column separately (Buddenbaum & Steffens, 2011; Steffens & Buddenbaum, 2013). Further preprocessing included masking the image areas that showed the subsections and applying a Savitzky–Golay spectral smoothing filter (filter width 11 spectral bands, polynomial order 2). A principal components transformation of the image data was calculated to compress the hyperspectral information into a few bands so that a maximum of information can be displayed in a three-band false-colour image.

We visually identified six information classes (fresh plant residues, undecomposed plant residues, decomposed POM, highly decomposed POM, Fe oxides and mineral matrix) in the reflected light microscopy image and transferred them to the imVisIR image. Training areas (one to three per class) were drawn in the B1-5U-2 image (Figure 1) to define the reference spectra for each class and this fixed set of reference spectra was used for the classification of both images (Figure 1). The spectra of the POM classes show a clear sequence of high to low reflectivity from fresh to highly decomposed POM (Ben-Dor, Inbar, & Chen, 1997). Fresh POM, undecomposed POM and decomposed POM have higher reflectance with larger wavelengths, whereas highly decomposed POM only reflects 1% of the incoming radiation across the whole wavelength region. The Fe oxides show a peak in the red wavelength region between 600 and 800 nm (Bartholomeus, Epema, & Schaepman, 2007). The mineral matrix covers most of the disks. Thus, mineral matrix spectra are quite diverse, but mostly flat, like the mean spectrum shown in Figure 1.

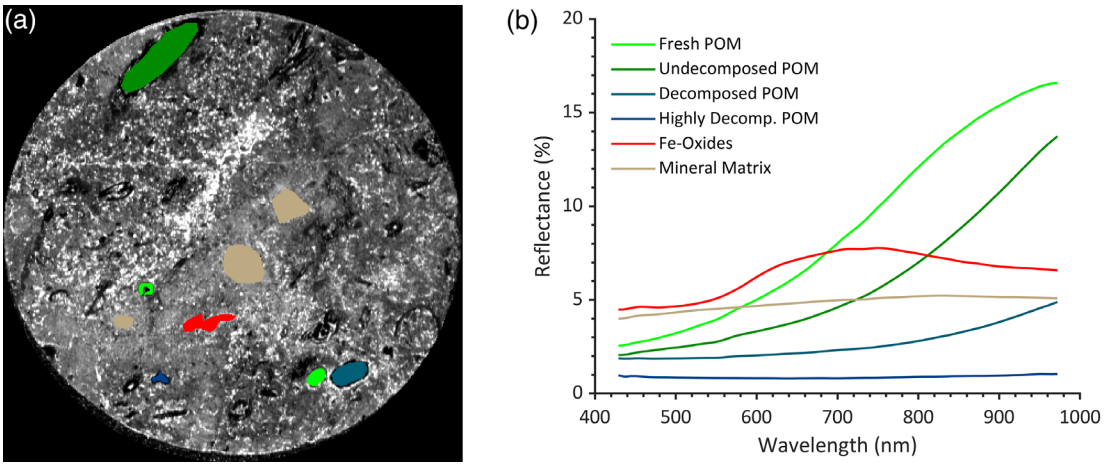


**FIGURE 1** Panel (a), training areas for supervised classification; panel (b), mean spectra of the information classes in the resin-embedded drill core subsection

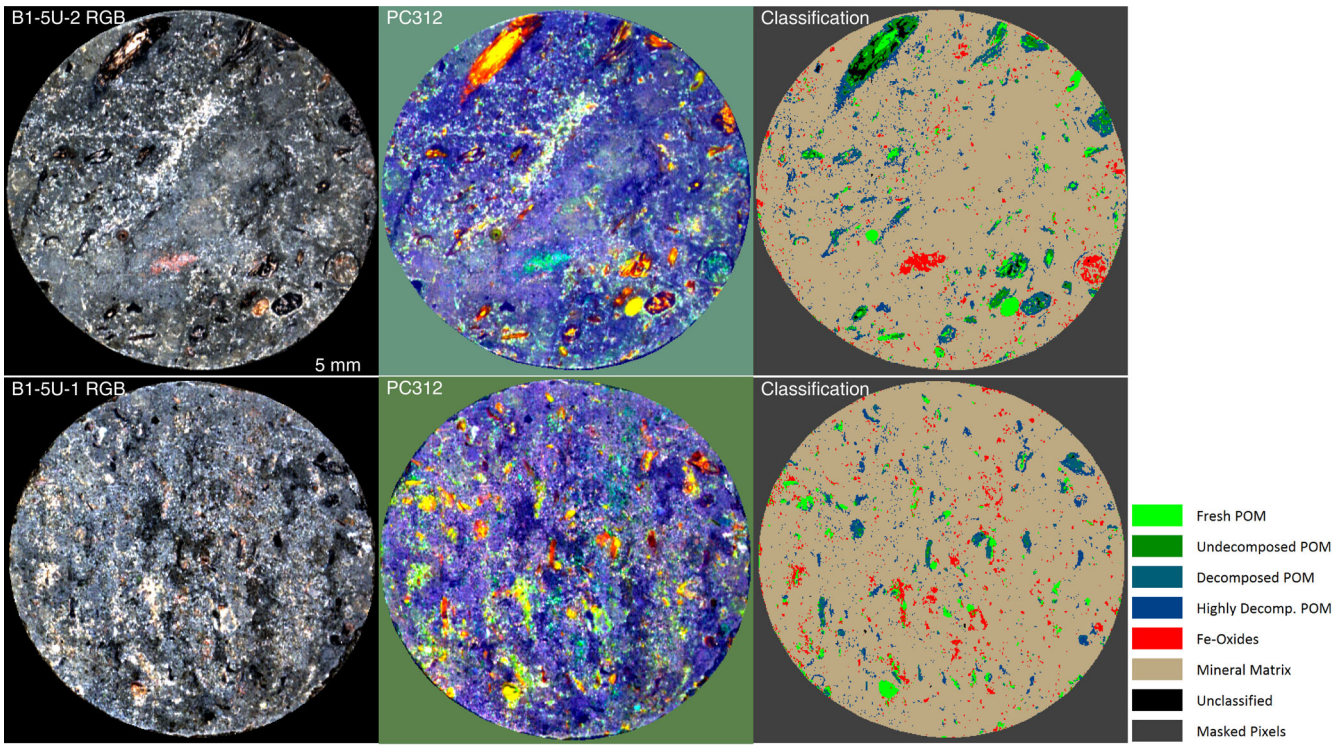


**FIGURE 2** Left: contrast-enhanced true-colour view of the two resin-embedded drill core subsections. Middle: red/green/blue composite of principal components 3, 1 and 2. Right: results of spectral angle mapper classifications

We conducted supervised spectral angle mapper (SAM) classifications in the image processing software Envi (Version 5.3, Exelis Visual Information Solutions, Gilching, Germany). Because two training areas for fresh POM and three areas for mineral matrix were defined in the pre-classification step, the classification process was conducted with nine spectral classes. In a post-classification step, the spectral classes were merged into the information classes mentioned above. The classification was transferred to disk B1-5U-1 by using the same training spectra and the same classification parameterization. A critical point of the present approach is the low number of two analysed core sections used to demonstrate the imaging and image classification workflow. Nevertheless, in contrast to most spectromicroscopic techniques the used imVisIR approach allows for a relatively high sample throughput and thus the creation of a spectral library of embedded soil core sections in the future. This will also include the implementation of

validation techniques (e.g., reflected light microscopy and laser ablation ICP-MS) to validate the soil constituents quantified using imVisIR.

Figure 2 shows a true-colour and a false-colour principal components depiction of both disks and the classification results. The frequency of the classes is depicted in Table 1. In both disks, the mineral matrix is the dominant constituent with 85 to 90% of the area. In total, POM covers 11.8% of the area of B1-5U-2 and 6.8% of the area of B1-5U-1, similar to the bulk soil analyses in Mueller et al. (2017). Only small parts are covered by fresh plant residues and Fe oxides, which nicely corresponds to the small-scale variability of soil constituents and processes in these permafrost samples. We can clearly demonstrate that the amount of POM (fresh and decomposed OM together with POM) and MOM (Fe-oxides and mineral matrix) quantified by our imaging approach on the two Cryosol sections (Table 1) corresponds very well with the amount of POM and MOM reported for the bulk soil sample (Mueller et al., 2017). Thus, the obtained data nicely demonstrate that imVisIR in combination with supervised image classification can be a tool that links measurements at the microscale (Mueller et al., 2017) with soil core (Mueller et al., 2015) and possibly also pedon data (Hobley, Steffens, Bauke, & Kögel-Knabner, 2018; Steffens & Buddenbaum, 2013). The successful transfer of classification training spectra from one resin-embedded drill core disk to another underlines the usefulness and transferability of the imVisIR approach, opening an avenue to implement microscale soil spectromicroscopy in larger-scale soil analyses. Also, in the reverse way, imVisIR, together with the easy to use supervised image classification, might be used to locate regions of interest in natural soil samples for subsequent fine-scale spectromicroscopic measurements.

## ACKNOWLEDGEMENTS

We thank Jenny Kao-Kniffin, James Bockheim and Kenneth Hinkel for the invitation to join the 2010 expedition and all the logistic assistance. We are grateful for assistance with fieldwork and sampling by Christine Mlot and the Barrow Arctic Science Consortium (BASC). The funding for the research was provided by the NSF Postdoctoral Fellowship in Polar Regions Research (#0852036). We are also grateful to the German Science Foundation (DFG) for the financial support in the frame of the "Initiation of International Collaboration" (MU 3021/2-1) and the funding within the DFG Priority Programme 1158 "Antarctic Research with Comparable Investigations in Arctic Sea Ice Areas" (MU 3021/8-1). H.B. was funded by the German Aerospace Center (DLR) and the German Federal Ministry of Economic Affairs and Energy in the framework of the EnMAP project, grant number 50 EE 1530.

## DATA AVAILABILITY STATEMENT

The data that support the findings of this study are available from the corresponding author upon reasonable request.

## ORCID

*Carsten W. Mueller* https://orcid.org/0000-0003-4119-0544
*Markus Steffens* https://orcid.org/0000-0002-2593-0971
*Henning Buddenbaum* https://orcid.org/0000-0002-0956-5628

## REFERENCES

Bartholomeus, H., Epema, G., & Schaepman, M. (2007). Determining iron content in Mediterranean soils in partly vegetated areas, using spectral reflectance and imaging spectroscopy. *International Journal of Applied Earth Observation and Geoinformation*, *9*, 194–203.

Baveye, P. C., Otten, W., Kravchenko, A., Balseiro-Romero, M., Beckers, É., Chalhoub, M., ... Vogel, H.-J. (2018). Emergent properties of microbial activity in heterogeneous soil microenvironments: Different research approaches are slowly converging, yet major challenges remain. *Frontiers in Microbiology*, *9*, 1929.

Ben-Dor, E., Inbar, Y., & Chen, Y. (1997). The reflectance spectra of organic matter in the visible near-infrared and short wave infrared region (400–2500 nm) during a controlled decomposition process. *Remote Sensing of Environment*, *61*, 1–15.

Buddenbaum, H., & Steffens, M. (2011). Laboratory imaging spectroscopy of soil profiles. *Journal of Spectral Imaging*, *2*, 1–5.

Buddenbaum, H., Watt, M. S., Scholten, R. C., & Hill, J. (2019). Preprocessing ground-based visible/near infrared imaging spectroscopy data affected by smile effects. *Sensors*, *19*, 1543.

Eickhorst, T., & Tippkoetter, R. (2008). Detection of microorganisms in undisturbed soil by combining fluorescence in situ hybridization (FISH) and micropedological methods. *Soil Biology & Biochemistry*, *40*, 1284–1293.

Gentsch, N., Mikutta, R., Shibistova, O., Wild, B., Schnecker, J., Richter, A., ... Guggenberger, G. (2015). Properties and bioavailability of particulate and mineral-associated organic matter in Arctic permafrost soils, lower Kolyma region, Russia. *European Journal of Soil Science*, *66*(4), 722–734. https://doi.org/10.1111/ejss.12269

Herrmann, A. M., Clode, P. L., Fletcher, I. R., Nunan, N., Stockdale, E. A., O'Donnel, A. G., & Murphy, D. V. (2007). A novel method for the study of the biophysical interface in soils using nano-scale secondary ion mass spectrometry. *Rapid Communications in Mass Spectrometry*, *21*, 29–34.

Herrmann, A. M., Ritz, K., Nunan, N., Clode, P. L., Pett-Ridge, J., Kilburn, M. R., ... Stockdale, E. A. (2007). Nano-scale secondary ion mass spectrometry — A new analytical tool in biogeochemistry and soil ecology: A review article. *Soil Biology and Biochemistry*, *39*, 1835–1850.

Hobley, E., Steffens, M., Bauke, S. L., & Kögel-Knabner, I. (2018). Hotspots of soil organic carbon storage revealed by laboratory hyperspectral imaging. *Scientific Reports*, *8*, 13900.

Juyal, A., Otten, W., Falconer, R., Hapca, S., Schmidt, H., Baveye, P. C., & Eickhorst, T. (2019). Combination of techniques to quantify the distribution of bacteria in their soil microhabitats at different spatial scales. *Geoderma*, *334*, 165–174.

Kravchenko, A. N., Guber, A. K., Razavi, B. S., Koestel, J., Quigley, M. Y., Robertson, G. P., & Kuzyakov, Y. (2019). Microbial spatial footprint as a driver of soil carbon stabilization. *Nature Communications*, *10*, 3121.

Kubiena, W. L. 1938. *Micropedology*. Ames, Iowa: Collegiate Press, 243.

Manß, J., Hilgers, C., Buddenbaum, H., & Stanjek, H. (2017). Visualising mineralogical heterogeneities and texture in a mudstone concretion using hyperspectral imaging. *Zeitschrift der Deutschen Gesellschaft für Geowissenschaften*, *168*, 403–414.

Mueller, C. W., Hoeschen, C., Steffens, M., Buddenbaum, H., Hinkel, K., Bockheim, J. G., & Kao-Kniffin, J. (2017). Microscale soil structures foster organic matter stabilization in permafrost soils. *Geoderma*, *293*, 44–53.

Mueller, C. W., Rethemeyer, J., Kao-Kniffin, J., Löppmann, S., Hinkel, K. M., & Bockheim, J. G. (2015). Large amounts of labile organic carbon in permafrost soils of northern Alaska. *Global Change Biology*, *21*(7), 2804-2817. https://doi.org/10.1111/gcb.12876

Mueller, C. W., Weber, P. K., Kilburn, M. R., Hoeschen, C., Kleber, M., & Pett-Ridge, J. (2013). Advances in the analysis of biogeochemical interfaces: NanoSIMS to investigate soil microenvironments. In D. L. Sparks (Ed.), *Advances in agronomy* (Vol. 121, pp. 1–46). Cambridge, MA: Academic Press.

Nunan, N., Ritz, K., Crabb, D., Harris, K., Wu, K. J., Crawford, J. W., & Young, I. M. (2001). Quantification of the in situ distribution of soil bacteria by large-scale imaging of thin sections of undisturbed soil. *FEMS Microbiology Ecology*, *37*, 67–77.

Rodionov, A., Lehndorff, E., Stremtan, C. C., Brand, W. A., Königshoven, H.-P., & Amelung, W. (2019). Spatial microanalysis of natural 13C/12C abundance in environmental samples using laser ablation-isotope ratio mass spectrometry. *Analytical Chemistry*, *91*, 6225–6232.

Rogass, C., Koerting, F. M., Mielke, C., Brell, M., Boesche, N. K., Bade, M., & Hohmann, C. (2017). Translational imaging spectroscopy for proximal sensing. *Sensors*, *17*, 1857.

Schaepman-Strub, G., Schaepman, M. E., Painter, T. H., Dangel, S., & Martonchik, J. V. (2006). Reflectance quantities in optical remote sensing—Definitions and case studies. *Remote Sensing of Environment*, *103*, 27–42.

Schlueter, S., Eickhorst, T., & Mueller, C. W. (2019). Correlative imaging reveals holistic view of soil microenvironments. *Environmental Science & Technology*, *53*, 829–837.

Schuur, E. A. G., Bockheim, J., Canadell, J. G., Euskirchen, E., Field, C. B., Goryachkin, S. V., ... Zimov, S. A. (2008). Vulnerability of permafrost carbon to climate change: Implications for the global carbon cycle. *Bioscience*, *58*, 701–714.

Schuur, E. A. G., McGuire, A. D., Schädel, C., Grosse, G., Harden, J. W., Hayes, D. J., ... Vonk, J. E. (2015). Climate change and the permafrost carbon feedback. *Nature*, *520*, 171–179.

Steffens, M., & Buddenbaum, H. (2013). Laboratory imaging spectroscopy of a stagnic luvisol profile - High resolution soil characterisation, classification and mapping of elemental concentrations. *Geoderma*, *195-196*, 122–132.

Steffens, M., Rogge, D. M., Mueller, C. W., Höschen, C., Lugmeier, J., Kölbl, A., & Kögel-Knabner, I. (2017). Identification of distinct functional microstructural domains controlling C storage in soil. *Environmental Science & Technology*, *51*, 12182–12189.

Tarnocai, C., Canadell, J. G., Schuur, E. A. G., Kuhry, P., Mazhitova, G., & Zimov, S. (2009). Soil organic carbon pools in the northern circumpolar permafrost region. *Global Biogeochemical Cycles*, *23*, 1–11.

Vaughn, L. J. S., & Torn, M. S. (2019). $^{14}C$ evidence that millennial and fast-cycling soil carbon are equally sensitive to warming. *Nature Climate Change*, *9*, 467–471.

Vidal, A., Hirte, J., Bender, S. F., Mayer, J., Gattinger, A., Höschen, C., ... Mueller, C. W. (2018). Linking 3D soil structure and plant-microbe-soil carbon transfer in the rhizosphere. *Frontiers in Environmental Science*, *6*, 1–14.

Zimov, S. A., Schuur, E. A. G., & Chapin, F. S. (2006). Permafrost and the global carbon budget. *Science*, *312*, 1612–1613.

**How to cite this article:** Mueller CW, Steffens M, Buddenbaum H. Permafrost soil complexity evaluated by laboratory imaging Vis-NIR spectroscopy. *Eur J Soil Sci*. 2020;1–6. https://doi.org/10.1111/ejss.12927